



Complex seismic anisotropy in the top of the Earth's inner core beneath Africa

Wen-che Yu¹ and Lianxing Wen¹

Received 21 November 2006; revised 25 April 2007; accepted 3 May 2007; published 7 August 2007.

[1] We report complex seismic anisotropy in the top 80 km of the Earth's inner core beneath Africa. The anisotropy in the top 80 km of the inner core is constrained using differential travel times, amplitude ratios, and waveforms of the PKiKP-PKIKP phases sampling Africa along various directions. The differential PKiKP-PKIKP time residuals (relative to the Preliminary Reference Earth Model [PREM]) along the polar paths are larger than those along the equatorial paths by 0–1.4 s, indicating the presence of seismic anisotropy in the top 80 km of the inner core. Furthermore, the observations along the polar paths show complex regional variations beneath Africa: the differential PKiKP-PKIKP travel time residuals vary from 1.2 s beneath eastern Africa, to –0.1 s beneath central Africa, and to –0.2 to 0.8 s beneath western Africa. A correlation between small PKIKP/PKiKP amplitude ratios and large differential PKiKP-PKIKP travel time residuals is observed. The waveform data are spatially binned into six groups to constrain the regional dependence of velocity and attenuation anisotropy in the top 80 km of the inner core. Overall, the seismic data can be explained by an isotropic upper inner core (UIC) overlying an anisotropic lower inner core (LIC) in the top 80 km of the inner core across Africa. The thickness of the isotropic UIC varies from 0 to 50 km, and the P velocity transition from the isotropic UIC to the anisotropic LIC is sharp, with velocity increases laterally varying from 1.6% to 2.2%. The attenuation structure along the polar paths has a Q value of 600 for the isotropic UIC and Q values varying from 150 to 400 for the anisotropic LIC. The complex seismic anisotropy in the top of the inner core is found in a region where a rapid change of the inner core boundary (ICB) between 1993 and 2003 was discovered (Wen, 2006) and may be explained by complex alignments of iron crystals, resulting from a localized anomalous solidification of the inner core.

Citation: Yu, W., and L. Wen (2007), Complex seismic anisotropy in the top of the Earth's inner core beneath Africa, *J. Geophys. Res.*, 112, B08304, doi:10.1029/2006JB004868.

1. Introduction

[2] Seismic anisotropy in the uppermost portion of the Earth's inner core is essential to our understanding of the dynamics and growth of the Earth's inner core. The inner core is anisotropic in both velocity and attenuation, with the direction of high velocity corresponding to that of high attenuation [Yu and Wen, 2006a]. The inner core anisotropy has an axial symmetry, with the symmetry axis being close to the Earth's rotation axis. It is generally believed that the inner core anisotropy results from the lattice preferred orientation of the anisotropic iron crystal [Takahashi and Bassett, 1964] or inclusion of melt [Singh *et al.*, 2000]. The proposed mechanisms to explain the inner core anisotropy are less clear, but they include the electromagnetic Maxwell

stresses [Karato, 1993, 1999; Buffett and Wenk, 2001], solidification texturing [Bergman, 1997], thermal convection [Jeanloz and Wenk, 1988; Romanowicz *et al.*, 1996; Wenk *et al.*, 2000], and viscous flow induced by preferential growth of the inner core in a certain direction [Yoshida *et al.*, 1996].

[3] Since Masters and Gilbert [1981] first identified the anomalous splitting of the normal modes that are sensitive to the inner core structures and Poupinet *et al.* [1983] observed the PKIKP travel time anomaly along the polar direction, there have been extensive studies on the seismic structures in the inner core. The inner core velocity anisotropy was first hypothesized about two decades ago by Morelli *et al.* [1986] and Woodhouse *et al.* [1986]. Both the normal modes of Earth's free oscillations and the body wave data suggest that the P velocity along the polar direction is higher than that along the equatorial direction by 3% (see reviews in Song [1997]; Creager [2000]; Tromp [2001]; Song [2003]; Souriau and Poupinet [2003]). Nevertheless, inner core velocity anisotropy exhibits an east-west hemispheric difference [Tanaka and Hamaguchi, 1997;

¹Department of Geosciences, State University of New York at Stony Brook, Stony Brook, New York, USA.

Creager, 1999; Garcia and Souriau, 2000; Niu and Wen, 2002]; and the uppermost 80 km of the inner core appears to have negligible or weak anisotropy [Shearer, 1994; Song and Helmberger, 1995, 1998; Niu and Wen, 2001, 2002; Ouzounis and Creager, 2001; Cao and Romanowicz, 2004]. The thickness of the uppermost isotropic layer appears to undulate from region to region: an isotropic layer of about 200 km beneath the eastern hemisphere (40°E–180°E) and of about 50–150 km beneath the western hemisphere (180°W–40°E) [Song and Helmberger, 1995, 1998; Ouzounis and Creager, 2001; Niu and Wen, 2001, 2002]. Song and Helmberger [1998] and Song and Xu [2002] proposed an inner core transition zone model with isotropic upper inner core (UIC) overlying anisotropic lower inner core (LIC). They further suggested that the separation of the UIC/LIC is sharp because of the triplications associated with the UIC/LIC boundary. Another change of anisotropic behavior near the innermost inner core (IMIC) was also proposed by Ishii and Dziewonski [2002] and Beghein and Trampert [2003], and waveform effects of the LIC/IMIC boundary were investigated by Cormier and Stroujkova [2005].

[4] Compared to the well-studied regions, such as those beneath Central America and the Caribbean Sea, the uppermost inner core beneath Africa has been less thoroughly studied. Here we study seismic anisotropic structures in the uppermost 80 km of the inner core beneath Africa, a region of particular interest. For instance, Wen [2006] analyzed a waveform doublet in the South Sandwich Islands and reported a localized change of the inner core boundary (ICB) beneath eastern and central Africa during the occurrence of the doublet. This region is also reported to exhibit anomalously strong small-scale magnetic field changes in the top of the inner core at present time [Hulot et al., 2002] and intensive secular variations in the Earth's magnetic field interpreted as rapidly drifting spots in the top of the outer core [Bloxxham and Gubbins, 1985]. In addition, Africa is close to the border of the inner core east-west hemispheric variations reported earlier by Tanaka and Hamaguchi [1997]; Creager [1999]; Garcia and Souriau [2000]; Niu and Wen [2001, 2002]; Garcia [2002]; Cao and Romanowicz [2004]; Stroujkova and Cormier [2004] and Yu and Wen [2006b]. The detailed seismic structure there would help us define the hemispheric border and better understand the anisotropy in the upper portion of the inner core.

2. Seismic Data and Coverage

[5] The waveforms of the PKIKP and PKiKP phases observed at the epicentral distance range of 120°–141° are used to constrain the seismic structures in the top 80 km of the Earth's inner core. PKIKP (PKP_{df}) is the *P*-wave transmitted in the inner core, and PKiKP (PKP_{cd}) is the *P*-wave reflected off the inner core boundary (ICB). Since the ray paths of the PKIKP and PKiKP phases are remarkably close in the mantle, the seismic heterogeneities in the mantle would affect the PKIKP and PKiKP phases in the same way (inset of Figure 1). The differential travel times of the PKiKP-PKIKP phases are insensitive to earthquake mislocation and the seismic heterogeneities in

the mantle. The PKIKP/PKiKP amplitude ratios are not very affected by the uncertainties on radiation patterns of the earthquake sources and by the attenuation structures in the mantle, as the PKiKP and PKIKP phases have nearly identical take-off angles and close ray paths in the mantle. The differential travel times, amplitude ratios, and waveforms of the PKiKP-PKIKP phases are thus most sensitive to the seismic velocity and attenuation structures in the top 80 km of the inner core.

[6] Our seismic data are assembled from the recordings in the Global Seismographic Network (GSN) of the Incorporated Research Institutions for Seismology (IRIS) Consortium for the period of 1990–2005 and in several regional seismic networks and temporary Program for the Array Seismic Studies of the Continental Lithosphere (PASSCAL) experiments: the GEOSCOPE, the GEOFON, the NORSAR in Norway, the FINES in Finland, Kazakhstan, Kyrgyzstan, the New China Digital Seismograph Network, the Tien Shan Continental Dynamics in China, the BLSP, the SEDA, the BANJO, and the Chile Argentina Experiment (CHARGE). We divide our data set into polar (defined as those in which the ray angle (ξ) between the PKIKP turning direction in the inner core and the Earth's rotation axis is smaller than 37°) and equatorial (defined as those in which the ray angle (ξ) between the PKIKP turning direction in the inner core and the Earth's rotation axis is greater than 37°) subsets (Figure 2b), as the travel time pattern changes near 37° from the Earth's rotation axis (gray dotted vertical line in Figure 2b). The polar subset is from earthquakes mostly occurring in the South Sandwich Islands recorded by the seismographs at high latitudes. The equatorial data are from earthquakes occurring in South America recorded by the seismographs in Asia or vice versa. Among the equatorial data set, the recordings of the BANJO, the SEDA, the BLSP, Kazakhstan, and Kyrgyzstan for the PKIKP sampling along the equatorial direction are collected from the previous studies [Niu and Wen, 2001; Wen and Niu, 2002; Yu and Wen, 2006b]. Broadband seismograms are band-pass filtered with the World-Wide Standard Seismograph Network (WWSSN) short-period instrument response. We select the data based on the simplicity of the earthquake source and high signal-to-noise ratio of the data (see Table 1 for the earthquake parameters for the polar data set). A total of 308 PKiKP-PKIKP high-quality observations sampling along polar paths are selected from more than 10,000 seismograms on the basis of the above criteria.

3. Seismic Observations and Models

3.1. Overall Observations

[7] The PKiKP-PKIKP differential travel times exhibit polar-equatorial differences for the PKIKP sampling the inner core beneath Africa (Figures 1 and 2a). The PKiKP-PKIKP differential travel time residuals relative to the Preliminary Reference Earth Model (PREM) [Dziewonski and Anderson, 1981] are about 0 s to 1.4 s larger for those along the polar paths than those along the equatorial paths. The negative differential travel time residuals observed beneath Africa are consistent with those in other areas of the western hemisphere observed previously (Figure 1 and Figure 1 of Niu and Wen [2001]), suggesting that Africa is

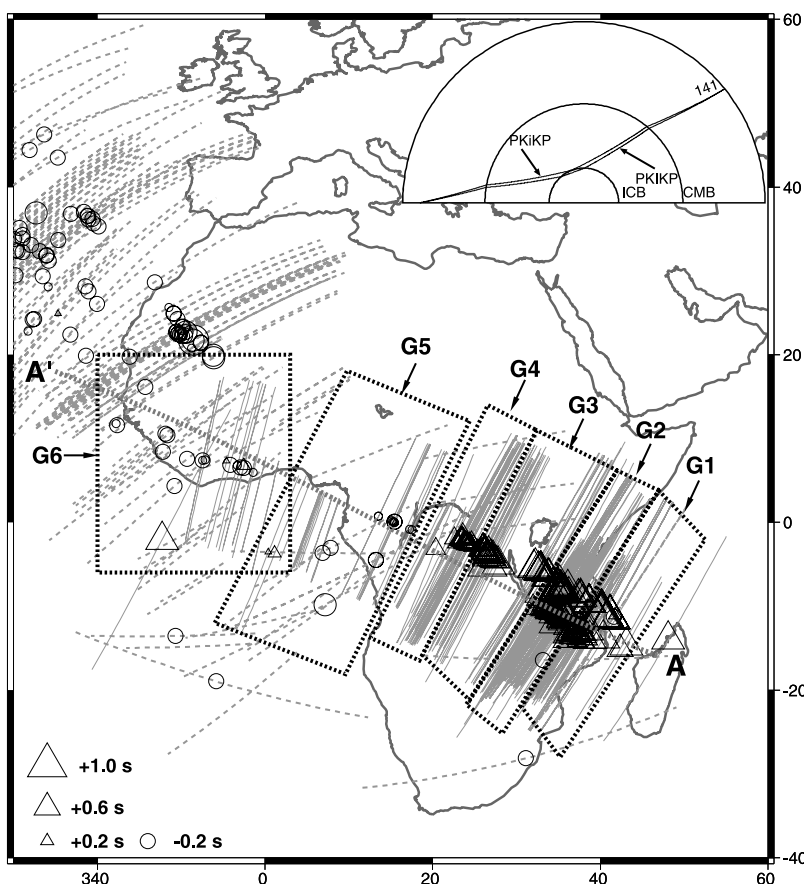


Figure 1. Map view of PKiKP-PKIKP differential travel time residuals with respect to PREM [Dziewonski and Anderson, 1981], along with the PKIKP ray segments in the inner core beneath Africa. Positive and negative differential travel time residuals are indicated by triangles and circles respectively, plotted at the PKIKP turning point in the inner core. The magnitude of the PKiKP-PKIKP differential travel time residuals is proportional to the size of the symbols. The legend is labeled in the left bottom of the figure. The PKIKP ray segments in the inner core sampling along the polar and equatorial directions are indicated by gray solid and gray dashed lines, respectively. The polar-path waveform data are spatially binned into six regions, labeled as G1 to G6, across Africa. The geographic divisions of these regions are framed with the dotted boxes. Raypaths of the PKiKP and PKIKP at an epicentral distance of 141° are shown in the inset. The profile of the polar velocity and attenuation models along the gray dotted line A-A' is shown in Figure 11.

within the geographic division of the western hemisphere. Therefore the polar-equatorial differences in differential travel time residuals indicate presence of seismic anisotropy in the top 80 km of the inner core beneath Africa. The observed differential travel time residuals, however, do not simply correlate with the ray angle and cannot be explained by a simple anisotropy model. Note that large differential time residuals are observed for the data within the ray angle (ξ) between 26° and 36° , whereas small differential time residuals are observed for those with their PKIKP ray angle (ξ) being smaller than 10° (Figure 2b). The differential PKiKP-PKIKP travel time residuals exhibit a lateral gradient across the PKIKP turning longitudes, decreasing laterally from 1.2 s to -0.1 s between 42°E and 30°E longitude, from 1.2 s to -0.1 s between 30°E and 15°E , and from 0.8 s to -0.2 s between 0°W and 20°W (Figure 2c). The PKiKP/PKIKP amplitude ratios also exhibit a similar complex lateral gradient, with small amplitude ratios corre-

lating with large differential travel time residuals (Figures 2c and 2d). The best fitting slope between PKiKP/PKIKP amplitude ratios (equivalent to attenuation) and PKiKP-PKIKP differential travel time residuals is about 0.7 s^{-1} . Such observations further support the hypothesis of inner core attenuation anisotropy [Souriau and Romanowicz, 1996, 1997; Yu and Wen, 2006a] and suggest complex anisotropy in the top of the inner core beneath Africa.

[8] The polar data are spatially binned into six groups in accordance with the complexities exhibited in the observations: G1 and G2 sampling the region of $30^\circ\text{E} - 40^\circ\text{E}$ of eastern Africa including Kenya, Tanzania, Mozambique; G3 and G4 sampling the region of $20^\circ\text{E} - 33^\circ\text{E}$ including Sudan, Uganda, the Democratic Republic of Congo, Zambia, Angola; G5 sampling the region from 16°E to 0°E including Cameroon, Nigeria, Congo; and G6 sampling western Africa (see Figure 1 for the geographic

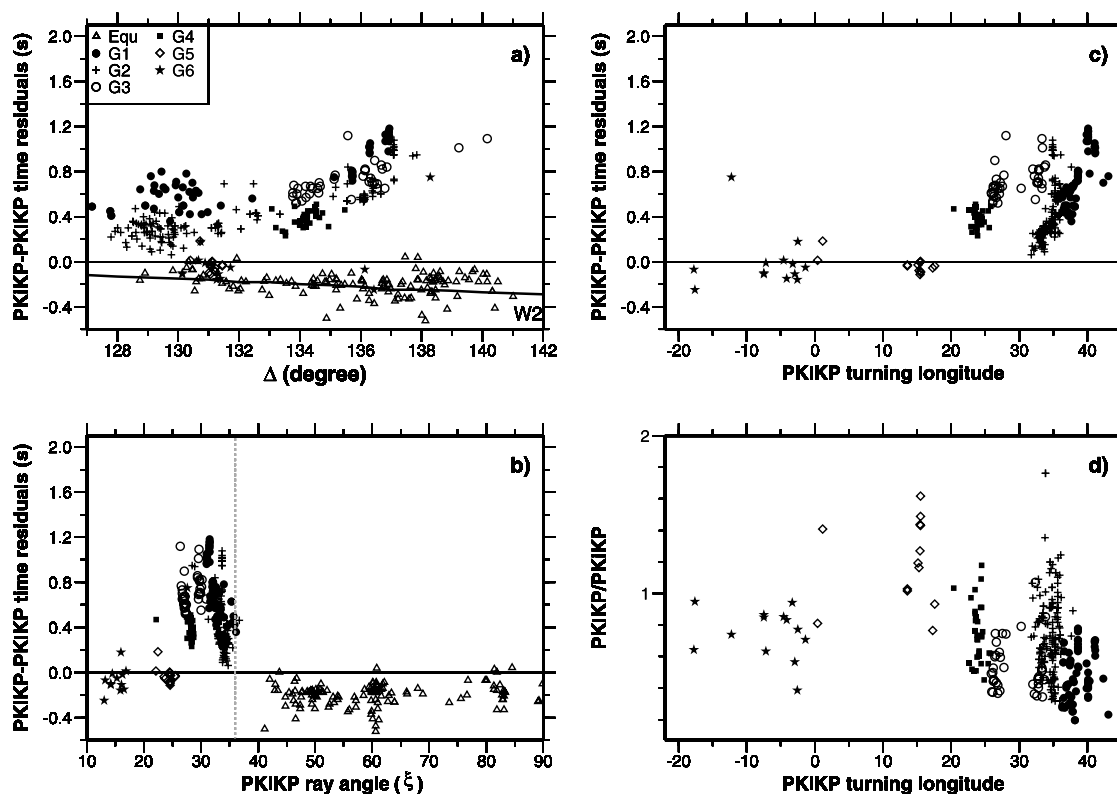


Figure 2. Differential PKiKP-PKIKP travel time residuals with respect to PREM as a function of (a) epicentral distance (Δ), (b) PKIKP ray angle (ξ), and (c) PKIKP turning longitude, and PKiKP/PKIKP amplitude ratios as a function of the PKIKP turning longitude (d). (a) and (b) include the seismic data sampling along the equatorial direction (open triangles, labeled with Equ). The polar path data include the following: G1, G2, G3, G4, G5, G6 (see Figure 1 for the geographic divisions of these regions). The legend is shown in the inset in (a). The predicted PKiKP-PKIKP differential travel time residuals based on the isotropic velocity model W2 for the western hemisphere [Wen and Niu, 2002; Yu et al., 2005; Yu and Wen, 2006b] (black solid line) are also plotted in (a). The differential travel time residuals and amplitude ratios show strong regional complexity (c, d) but less direction dependence (b). A correlation between large (small) PKiKP-PKIKP differential travel time residuals and small (large) PKiKP/PKIKP amplitude ratios is observed (c, d).

divisions and Figures 2–10 for the data). In what follows, we discuss in detail how the grouped waveforms are used to constrain the detailed velocity and attenuation structures in the top 80 km of the inner core along the polar paths for these regions.

3.2. Seismic Velocity and Attenuation Structures Along Polar Paths

3.2.1. Overall Approach

[9] The anisotropic velocity and attenuation models beneath Africa are inferred in comparison with the isotropic velocity and attenuation models W2. The isotropic velocity model W2 for the western hemisphere in the top 400 km of the inner core is derived from the joint modeling of the PKiKP-PKIKP waveforms and the PKPbc-PKIKP differential travel times [Wen and Niu, 2002; Yu et al., 2005; Yu and Wen, 2006b]. The isotropic velocity model W2 has a P velocity increase of 0.645 km/s across the ICB and a velocity gradient of 0.049 (km/s)/100 km in the top 375 km. The isotropic attenuation model W2, derived from

fitting the PKIKP amplitudes, has an average Q value of 600 in the top 400 km of the inner core (Figure 6 of Yu and Wen [2006b]).

[10] The PKiKP-PKIKP waveforms are used to constrain the velocity and attenuation structures in the top of the inner core. The bifurcation of the PKiKP-PKIKP phases (the onset of the visual separation of the PKIKP phase from the PKiKP phase in the short-period seismograms) can be used to constrain the P velocity increase across the ICB. Bifurcation occurring at a smaller distance indicates a larger P velocity increase across the ICB and vice versa. For a model of an isotropic UIC overlying anisotropic LIC separated by a first-order velocity discontinuity, a smaller bifurcation distance indicates a thinner isotropic layer in the top and/or a larger P velocity increase across the UIC/LIC boundary. The subsequent move-out of the PKiKP-PKIKP phases is sensitive to the radial velocity gradient in the top 80 km of the inner core. Synthetic waveforms are computed using the generalized ray theory method [Helmberger, 1983].

Table 1. South Sandwich Islands Events Used in This Study

No.	Origin Date	Origin Time (UT)	Latitude, °N	Longitude, °E	Depth, km	Magnitude
19900509	1990/05/09	04:21:10	-56.38	-27.06	33	6.0
19920320	1992/03/20	18:45:09	-56.43	-27.12	105	5.8
19920525	1992/05/25	20:51:09	-54.60	-30.26	33	5.8
19920622	1992/06/22	04:00:41	-60.73	-21.97	12	6.0
19920824	1992/08/24	19:40:34	-56.62	-26.55	107	5.9
19921121	1992/11/21	23:11:50	-56.32	-25.88	33	5.4
19930427	1993/04/27	13:04:05	-55.67	-27.14	33	5.5
19930909	1993/09/09	21:52:12	-56.21	-27.33	110	5.8
19931201	1993/12/01	00:59:01	-57.47	-25.68	33	5.5
19940725	1994/07/25	04:39:17	-56.97	-25.50	33	5.6
19940810	1994/08/10	14:57:49	-58.76	-25.54	33	5.6
19950103	1995/01/03	02:54:57	-56.21	-27.28	130	5.5
19950103	1995/01/03	16:11:57	-57.70	-65.88	14	6.2
19950407	1995/04/07	10:02:00	-56.70	-26.73	90	5.1
19950417	1995/04/17	08:52:20	-55.66	-27.42	33	5.2
19950530	1995/05/30	16:56:24	-60.23	-31.55	33	5.4
19950818	1995/08/18	02:16:26	-55.93	-28.83	42	5.7
19951106	1995/11/06	04:31:43	-55.28	-29.24	33	5.3
19951120	1995/11/20	15:48:39	-60.69	-24.81	33	4.7
19960123	1996/01/23	01:19:43	-61.06	-25.96	33	4.8
19960523	1996/05/23	03:38:42	-56.00	-27.78	137	5.1
19960530	1996/05/30	03:04:37	-56.72	-26.31	84	5.7
19960616	1996/06/16	00:06:17	-60.28	-26.29	33	5.2
19970214	1997/02/14	23:43:43	-56.37	-27.40	143	5.4
19970402	1997/04/02	03:04:40	-58.26	-25.46	33	4.9
19970529	1997/05/29	00:12:30	-55.65	-26.81	33	5.2
19970602	1997/06/02	21:24:38	-57.78	-25.47	33	5.9
19970615	1997/06/15	13:01:10	-56.85	-24.96	33	5.0
19970810	1997/08/10	22:03:31	-56.23	-27.19	94	5.3
19971005	1997/10/05	18:04:30	-59.74	-29.20	274	6.0
19971120	1997/11/20	06:08:10	-59.06	-25.51	33	5.2
19971214	1997/12/14	08:59:07	-55.80	-26.88	33	5.0
19980113	1998/01/13	08:49:12	-55.52	-28.20	33	5.5
19980206	1998/02/06	13:01:16	-56.06	-27.71	129	5.5
19980520	1998/05/20	06:17:52	-56.15	-27.57	105	4.7
19980730	1998/07/30	23:36:31	-58.81	-25.27	33	5.1
19980809	1998/08/09	20:03:30	-58.77	-25.35	33	4.9
19980901	1998/09/01	10:29:49	-58.21	-26.53	152	5.4
19981027	1998/10/27	16:47:47	-56.08	-26.71	33	4.9
19990403	1999/04/03	00:31:38	-57.68	-27.08	150	5.0
19990521	1999/05/21	03:12:17	-60.79	-24.95	40	4.9
19990622	1999/06/22	18:48:17	-56.27	-27.64	95	5.4
19991018	1999/10/18	02:43:23	-56.12	-26.58	33	6.0
20000502	2000/05/02	15:49:13	-58.81	-26.56	128	4.7
20000813	2000/08/13	07:44:10	-61.09	-24.64	33	4.7
20000911	2000/09/11	10:03:13	-57.73	-25.14	33	5.4
20001022	2000/10/22	11:37:24	-57.24	-25.42	33	5.3
20001112	2000/11/12	03:29:57	-55.36	-29.90	33	5.3
20010808	2001/08/08	18:07:30	-56.00	-27.68	115	5.1
20011001	2001/10/01	04:18:15	-58.31	-25.44	33	5.5
20020210	2002/02/10	01:47:06	-55.91	-29.00	193	5.7
20020309	2002/03/09	12:27:11	-56.02	-27.33	118	5.8
20020730	2002/07/30	06:55:07	-57.89	-23.24	33	5.7
20020907	2002/09/07	18:08:37	-57.92	-24.99	33	5.1
20021004	2002/10/04	12:37:16	-57.35	-26.29	150	5.1
20021112	2002/11/12	01:46:49	-56.55	-27.54	120	6.0
20021218	2002/12/18	01:47:07	-57.00	-25.20	10	5.1
20030207	2003/02/07	06:34:03	-56.29	-26.99	85	5.4
20030519	2003/05/19	00:21:36	-60.08	-26.90	33	5.5
20030804	2003/08/04	18:18:30	-60.59	-43.04	10	5.3
20030906	2003/09/06	15:46:59	-57.42	-25.64	33	5.6
20030920	2003/09/20	17:38:34	-55.88	-27.91	116	5.5
20031020	2003/10/20	16:50:18	-58.09	-26.25	156	5.4
20031029	2003/10/29	19:54:19	-60.57	-25.30	33	5.4
20031107	2003/11/07	21:21:29	-57.05	-25.70	33	5.0
20040505	2004/05/05	20:59:40	-57.19	-25.41	53	5.1
20040507	2004/05/07	09:50:31	-57.91	-25.53	71	5.1
20040730	2004/07/30	12:14:33	-57.26	-25.80	61	5.4
20040827	2004/08/27	20:26:54	-57.62	-25.60	64	5.1
20041008	2004/10/08	15:28:39	-56.53	-26.87	101	5.6
20041026	2004/10/26	20:48:14	-57.07	-24.83	10	5.4
20041112	2004/11/12	02:54:52	-59.75	-27.90	126	5.1
20041118	2004/11/18	03:22:57	-55.16	-29.06	44	4.7

Table 1. (continued)

No.	Origin Date	Origin Time (UT)	Latitude, °N	Longitude, °E	Depth, km	Magnitude
20050526	2005/05/26	23:29:29	-59.66	-27.56	139	5.1
20050804	2005/08/04	12:11:20	-59.77	-25.89	45	5.7
20050826	2005/08/26	21:42:06	-59.51	-28.38	272	4.8

3.2.2. Region G1

[11] The polar PKiKP-PKIKP waveforms for the seismic data sampling region G1 show that (1) the PKiKP-PKIKP phases bifurcate less than 127° ; (2) the PKIKP phases arrive about 0.5 s to 1.2 s earlier than the predictions based on PREM at the distance range of 127° – 137° ; and (3) the polar PKIKP amplitudes are smaller than the equatorial PKIKP amplitudes (see observations in Figure 3c; also Figures 3 and 5 of Wen and Niu [2002] for the equatorial PKiKP-PKIKP data sampling the western hemisphere).

[12] For G1, synthetics based on a velocity model with a P velocity increase across the ICB larger than that of W2 by 2.0% and the W2 velocity gradient in the top 100 km of the inner core can explain the time separation between the PKiKP and PKIKP phases at the distance of 127° and the subsequent move-out of the PKiKP-PKIKP phases, respectively (G11 velocity model, black solid line in Figure 3a; G11 synthetics, solid traces in Figure 3d). Waveform modeling of the seismic data suggests that the top isotropic layer should be less than 20 km. Synthetics based on an isotropic layer with a thickness of 20 km or larger would predict a bifurcation distance after 128° (see G31 synthetics in Figure 5d; G31 velocity model and synthetics will be discussed later in section 3.2.4), different from what is observed in the data (Figure 3c). With the top isotropic layer constrained to be less than 20 km, we search for the best fitting models within a range of these model parameters: the allowable thickness of the top isotropic layer, the P velocity increase across the UIC/LIC boundary, and the velocity gradient below. For a model with an isotropic layer in the top 10 km of the inner core, synthetics based on a P velocity increase of 2.2% at the UIC/LIC boundary, and the W2 velocity gradient in the LIC (G12 velocity model, black dashed line in Figure 3a; G12 synthetics, dashed traces in Figure 3d) are indistinguishable from G11 synthetics on the basis of fitting the observations.

[13] The attenuation model for G1 is inferred from the velocity model that best explains the PKiKP-PKIKP waveforms. For a uniform anisotropy velocity model G11, synthetics based on an average Q value of 200 can explain the observed PKIKP amplitudes (G11 attenuation model, solid line in Figure 3b; G11 synthetics in Figure 3d). For a model with a 10-km-thick isotropic layer, G12 synthetics based on a Q value of 600 in the top 10 km and a Q value of 200 in the deeper portion of the inner core can explain the observed PKIKP amplitudes equally well (G12 attenuation model, dashed line in Figure 3b; G12 synthetics in Figure 3d).

[14] For region G1, the seismic velocity structure along polar paths has an isotropic layer of 0–10 km; the seismic velocity structure along polar paths is uniformly higher than that along equatorial paths by 2.0%–2.2%; and the attenuation structure along polar paths has an average Q value of 200 (Figures 3a and 3b).

3.2.3. Region G2

[15] The polar PKiKP-PKIKP waveforms for the seismic data sampling region G2 show that (1) the PKiKP-PKIKP phases bifurcate less than 128° ; (2) the PKIKP phases arrive about 0.2 s to 1.0 s earlier than the predictions based on PREM at the distance range of 128° – 138° ; and (3) the polar PKIKP amplitudes are smaller than the equatorial PKIKP amplitudes (Figure 4c). The thickness of the top isotropic layer in this region should also be less than 20 km, following the same line of argument for the G1 observations. For a velocity model without an isotropic layer in the top of the inner core, synthetics based on a velocity model with a P velocity increase across the ICB larger than that of W2 by 1.4%, followed by the W2 velocity gradient in the top portion of the inner core, can explain the PKiKP-PKIKP move-out at the distance range of 128° – 137° (G21 velocity model, black solid line in Figure 4a; G21 synthetics, solid traces in Figure 4d). An average Q value of 400 (G21 attenuation model, solid line in Figure 4b) can explain the observed PKIKP amplitudes (G21 synthetics in Figure 4d). For a velocity model with a 10-km-thick isotropic layer in the top of the inner core, synthetics based on a velocity model with a P velocity increase of 1.6% at the UIC/LIC boundary, and the W2 velocity gradient in the LIC (G22 velocity model, black dashed line in Figure 4a) and an attenuation model with a Q value of 600 in the UIC and a Q value of 400 in the LIC (G22 attenuation model, dashed line in Figure 4b; G22 synthetics, dashed traces in Figure 4d) are indistinguishable from G21 synthetics on the basis of fitting the observations.

[16] Beneath G2, the seismic anisotropic velocity structure has an isotropic layer of 0–10 km and a velocity anisotropy of about 1.4%–1.6%; and the anisotropic attenuation structure has an average Q value of 400 (Figures 4a and 4b).

3.2.4. Region G3

[17] The polar PKiKP-PKIKP waveforms for the seismic data sampling region G3 show that (1) the PKiKP-PKIKP phases bifurcate at a distance of 128° ; (2) the PKIKP phases arrive about 0.6 s to 1.1 s earlier than the predictions based on PREM at the distance range of 134° – 140° ; (3) the polar PKIKP amplitudes are smaller than the equatorial PKIKP amplitudes; and (4) secondary arrivals after the PKIKP are observed (we term them “the post PKIKP phases”) (Figure 5c). The thickness of the isotropic UIC beneath G3 is about 20 km, inferred from the bifurcation distance of 128° . Synthetics based on a velocity model with a 30-km-thick isotropic layer would predict a bifurcation distance of 129° (see G41 synthetics, solid traces in Figure 8d; we will discuss G41 velocity model and synthetics in section 3.2.5). Synthetics based on a velocity model with a 20-km-thick UIC, followed by a first-order velocity discontinuity of

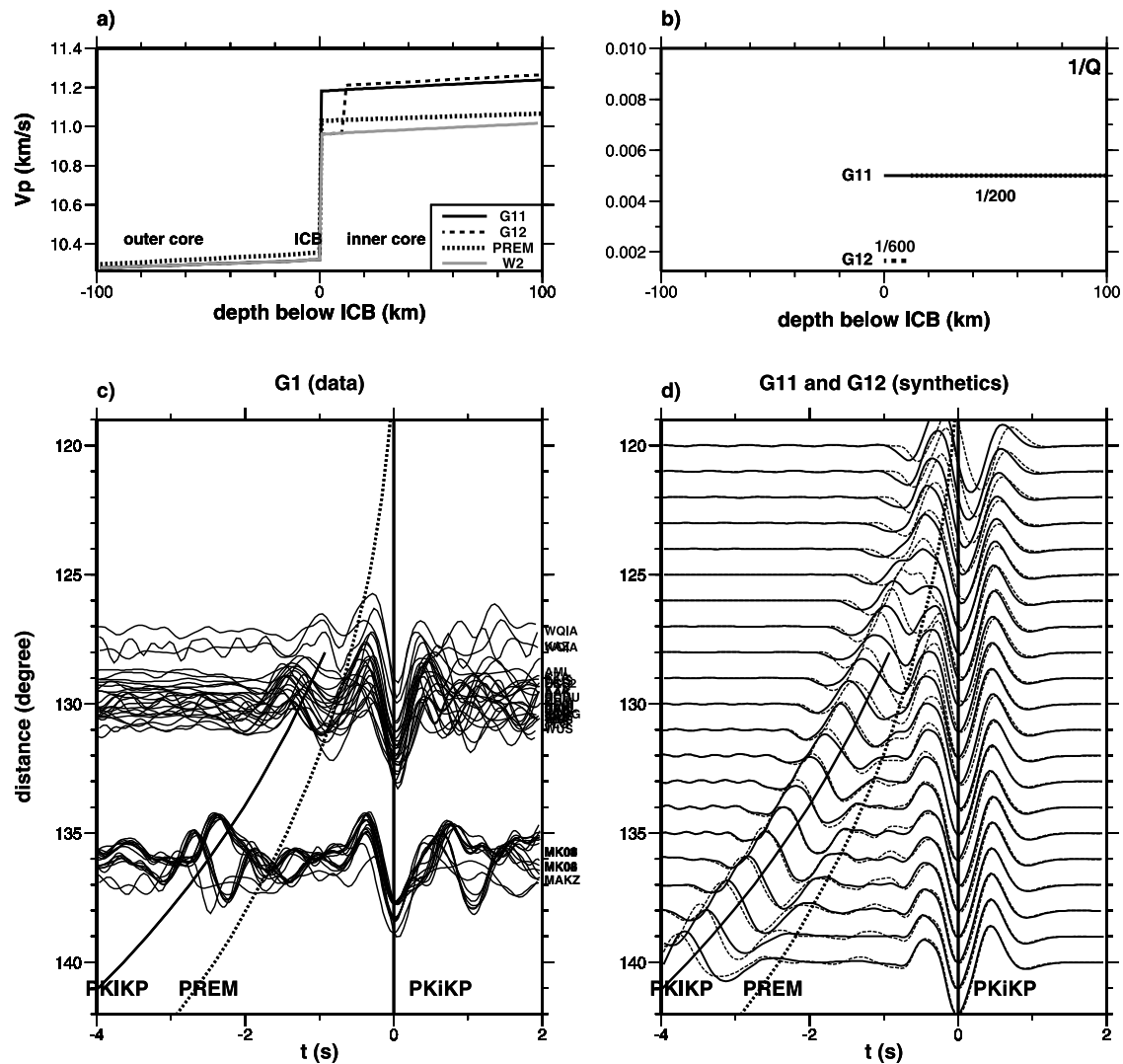


Figure 3. Compressional polar velocity (a) and attenuation (b) models of G11 and G12 near the ICB for region G1; observed waveforms for the PKIKP and PKiKP phases sampling G1 along polar paths (c); synthetic waveforms computed based on G11 (solid traces) and G12 (dashed traces) (d). PREM and W2 are also shown in (a). The velocity model G11 has a P velocity increase across the ICB with a magnitude of 2.0% larger than that of W2, and the W2 velocity gradient in the top 100 km of the inner core (black solid line in (a)); the attenuation model G11 has an average Q value of 200 in the top 100 km of the inner core (solid line labeled with G11 in (b)). G12 has a top isotropic layer of 10 km, a P velocity increase of 2.2% larger than W2, and the W2 velocity gradient in the deeper part of the inner core (dashed line in (a)); the attenuation model G12 has a Q value of 600 in the top 10 km and a Q value of 200 in the deeper part of the inner core (dashed line labeled with G12 in (b)). Distance corrections are made such that each trace is aligned at the distance equivalent to a source depth of 600 km. The predicted PKiKP arrivals are also based on a source depth of 600 km (dotted line for PREM; solid line for G11) (c, d). The observed and synthetic waveforms are aligned according to the maximum PKiKP amplitudes. G11 synthetics (solid traces in (d)) cannot be distinguished from G12 synthetics (dashed traces in (d)) on the basis of fitting the observations (c).

2.0% at the UIC/LIC boundary, and the W2 velocity gradient in the LIC match well the PKiKP-PKIKP waveforms observed at the bifurcation distance and the subsequent move-out at greater distances (G31 velocity model, black solid line in Figure 5a; G31 synthetics, solid traces in Figure 5d). The attenuation model is assumed to have a layered UIC/LIC structure. With a Q value of 600 in the 20-km-thick UIC, synthetics based on an average

Q value of 150 in the LIC are required to account for the observed PKiKP amplitudes at larger distances (G31 attenuation model, solid line in Figure 5b; G31 synthetics in Figure 5d).

[18] Beneath G3, the isotropic UIC is 20 km thick; the boundary between the isotropic UIC and anisotropic LIC is sharp, with a P velocity increase of 2.0%; and the attenuation structure has a Q value of 600 for the isotropic UIC

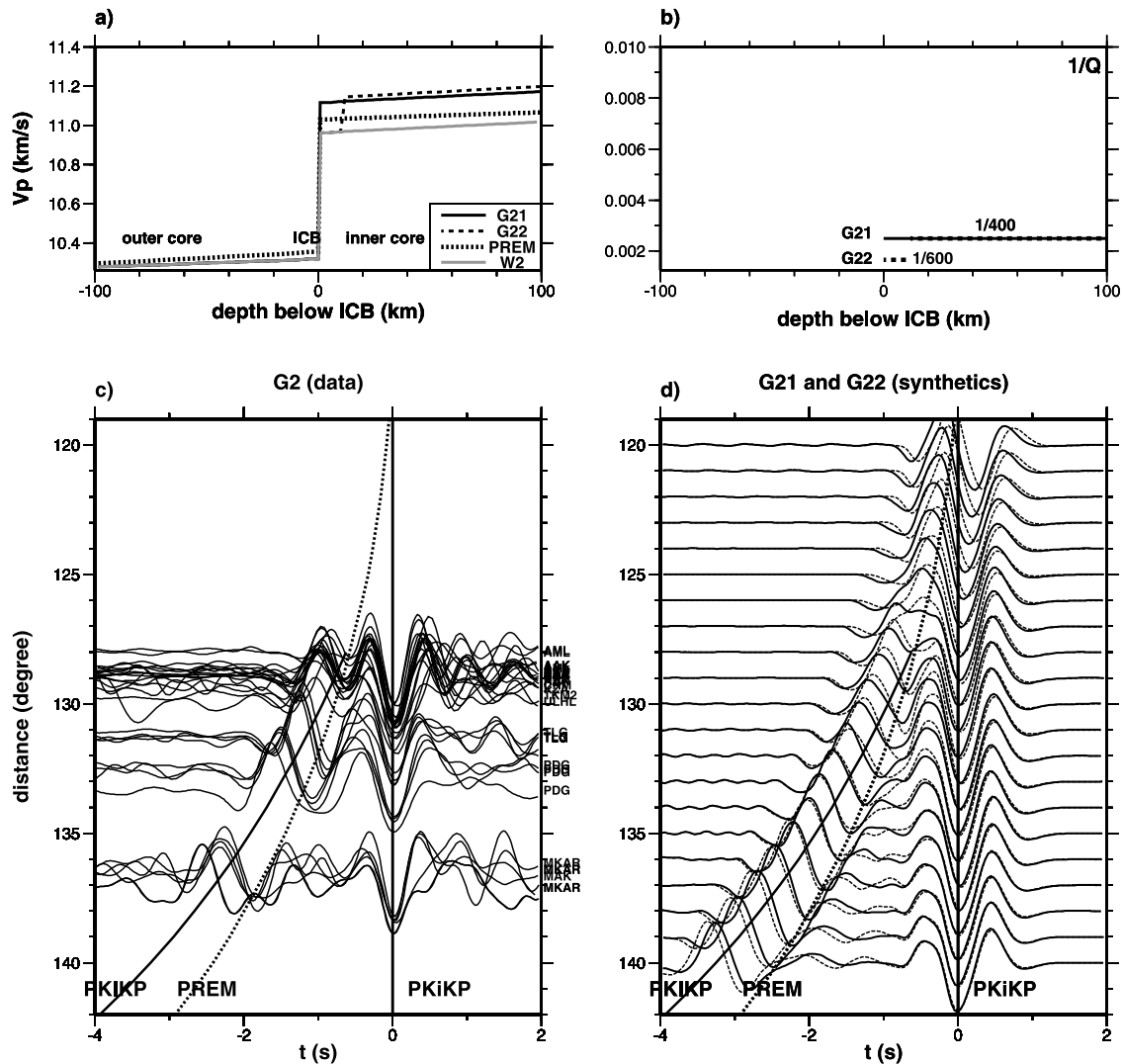


Figure 4. Seismic polar velocity (a) and attenuation (b) models of G21 and G22 near the ICB for region G2; observed PKiKP-PKiKP waveforms for the PKiKP sampling G2 along the polar paths (c); synthetics computed based on G21 (solid traces) and G22 (dashed traces) (d). The velocity model G21 has a P velocity increase across the ICB larger than that of W2 by 1.4%, and the W2 velocity gradient in the top 100 km of the inner core (black solid line in (a)); the attenuation model G21 has an average Q value of 400 in the top 100 km of the inner core (solid line labeled with G21 in (b)). The velocity model G22 has an isotropic layer in the top 10 km, followed by a P velocity increase of 1.6%, and the W2 velocity gradient in the deeper part of the inner core (dashed line in (a)); the attenuation model G22 has a Q value of 600 in the top 10 km and a Q value of 400 in the deeper part of the inner core (dashed line labeled with G22 in (b)). Distance corrections, synthetics, and the predicted PKiKP arrivals based on PREM (dotted line) and G21 (solid line) are made on the basis of a source depth of 600 km (c, d). The observations and synthetics are aligned according to the maximum PKiKP amplitudes (c, d). G21 synthetics (solid traces in (d)) cannot be distinguished from G22 synthetics (dashed traces in (d)) on the basis of fitting the observations (c).

and a Q value of 150 for the anisotropic LIC (Figures 5a and 5b).

[19] Seismic data from other earthquakes and recorded at other stations suggest that the post PKiKP phases cannot be caused by complex earthquake sources or localized structure beneath seismic stations. The earthquake source effects should be recorded in all seismic stations, whereas the signals from the seismic stations should be independent of the location and focal mechanism of the earthquake source.

Figure 6 compares four events recorded by the GSN, Kazakhstan, Kyrgyzstan, and the Canadian National Seismograph Network (CNSN) stations. Stations BRVK, CHK, CHKZ, KUR, KURK, and VOS consistently exhibit the post PKiKP phases (solid traces marked with black dotted bars) for all four events, while such signals are not observed in the CNSN stations FRB, CBB, LLLB, RES, YKW, the GSN station ALE, and the Kyrgyzstan station PDG for the same earthquake (dashed traces). Figure 7 compares obser-

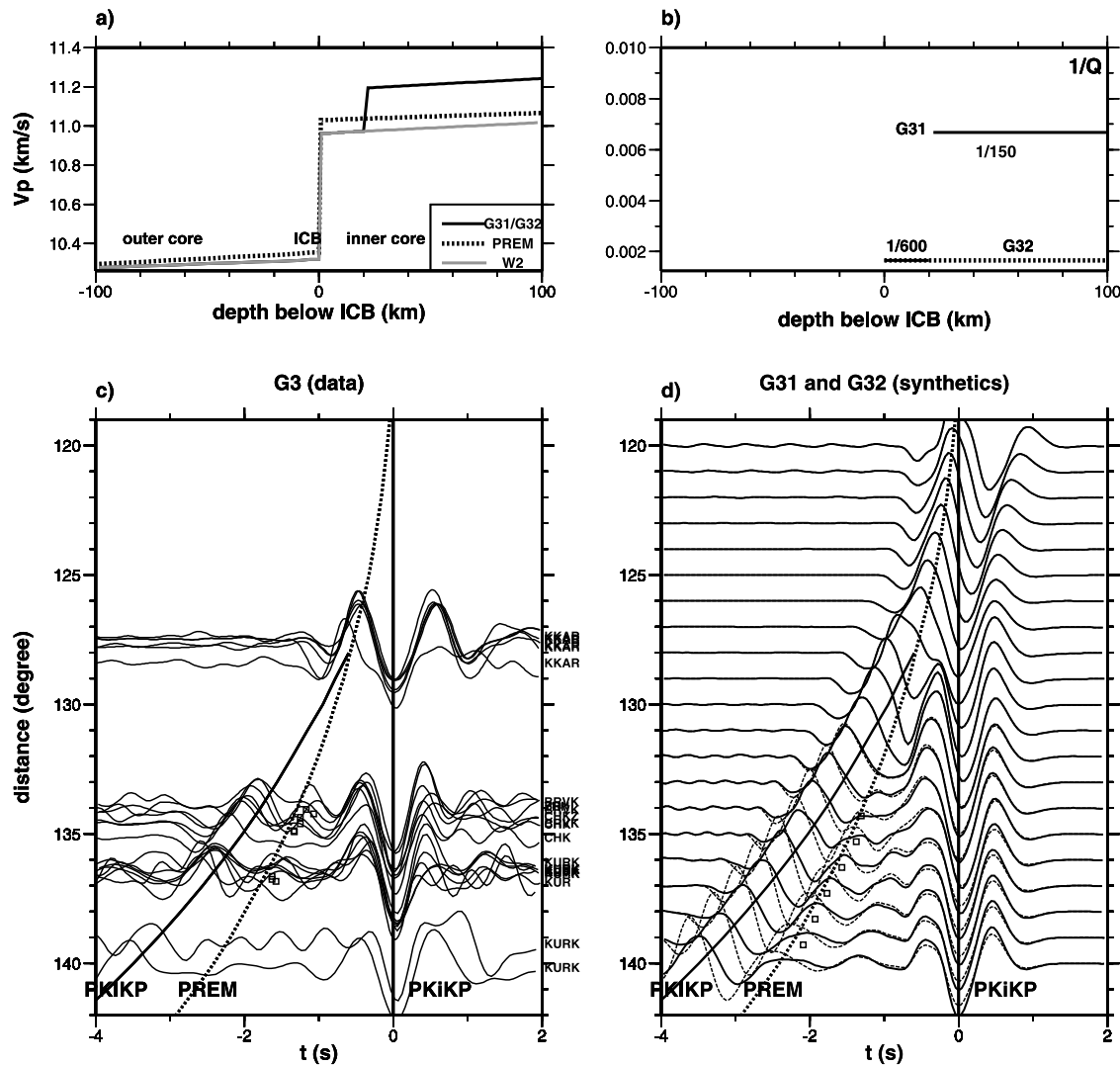


Figure 5. Seismic polar velocity (a) and attenuation (b) models G31 and G32 near the ICB for region G3; observed polar PKiKP-PKiKP waveforms sampling G3 (c); synthetics based on G31 (solid traces) and G32 (dashed traces) (d). PREM and W2 are also shown in (a). The velocity models G31 and G32 have a 20-km-thick isotropic upper inner core (UIC), followed by a P velocity increase of 2.0% at the isotropic UIC and anisotropic lower inner core (LIC) boundary, and the W2 velocity gradient in the LIC (black solid line in (a)); the attenuation model G31 has a Q value of 600 in the top 20 km and an average Q value of 150 in the deeper portion of the inner core (solid line labeled with G31 in (b)); the attenuation model G32 has a Q value of 600 in the top 100 km of the inner core (dashed line labeled with G32 in (b)). Distance corrections, synthetics, and the predicted PKiKP arrivals based on PREM and G31 (solid line) are also made on the basis of a source depth of 600 km (c, d). The observations and synthetics are aligned according to the maximum PKiKP amplitudes (c, d). The maximum amplitudes of the triplicated phases are marked by open squares.

vations recorded in five seismographic stations, ARU, BRVK, CHK, KURK, OBN for eleven South Sandwich Islands events (solid traces) and twelve South America events (dashed traces). At stations BRVK, CHK, KURK, the post PKiKP signals (marked with black dotted bars) are consistently observed for the South Sandwich Islands events, but such phases are absent for the seismic data recorded for the South America events (dashed traces). The observed post PKiKP phases thus cannot be caused by source or localized station effects.

[20] The post PKiKP signals most likely originated from the triplications from the inner core structure. The move-out of the triplications matches well those in G31 synthetics (triplicated phases are marked with open squares in Figures 5c and 5d), but they cannot be reconciled with one-dimensional models. A lower attenuation in the inner core would predict larger amplitudes for both the PKiKP and the triplicated phases and cannot explain the relative amplitudes of these phases. For instance, the amplitudes of the triplicated phases in G32 synthetics based on an atten-

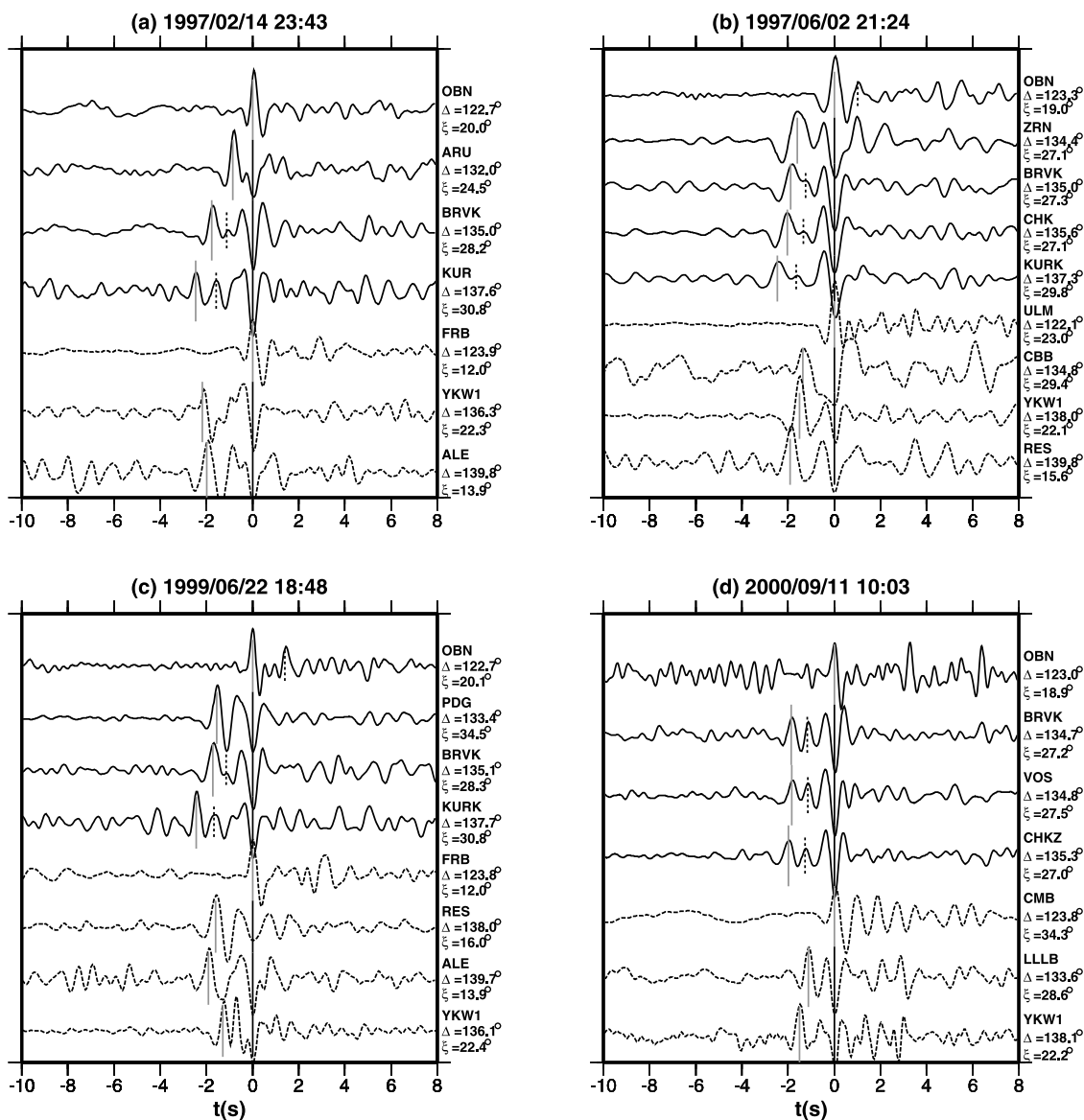


Figure 6. Observed PKIKP and PKiKP phases sampling Africa (solid traces) and the middle Atlantic Ocean, Central America, and the Caribbean Sea (dashed traces) along polar paths, selected from four South Sandwich Islands events: (a) 1997/02/14 23:43 UT, (b) 1997/06/02 21:24 UT, (c) 1999/06/22 18:48 UT, and (d) 2000/09/11 10:03 UT (see Table 1 for the earthquake parameters). The maximum amplitudes of the PKiKP and PKiKP phases are marked by gray and black bars, respectively, whereas the post PKiKP phases are marked by black dotted bars. Seismographic station name, epicentral distance (Δ), and the PKiKP ray angles (ξ) are labeled in the right. Note that the post PKiKP phases are consistently observed at stations BRVK, CHK, CHKZ, KUR, KURK, and VOS for the PKiKP sampling G3 and G4, while such phases are not observed for ALE, CMB, and the CNSN stations for the same earthquake.

uation model with a Q value of 600 in the top 100 km of the inner core, though larger than those based on G31 synthetics, are still smaller than the observations (G32 synthetics, dashed traces in Figure 5d). On the other hand, the PKiKP amplitudes in G32 synthetics are much larger than those in the observations. While the magnitude of the P velocity increase at the UIC/LIC boundary and/or the depth of the UIC/LIC reflector can be adjusted to explain the observed amplitudes of the triplicated phases at the distance

range of 134° – 135° , such modifications would produce unacceptable misfits to the subsequent move-out of the PKiKP-PKiKP phases and the triplications. The observed large amplitudes of the triplicated phases at the distance range of 134° – 135° remain enigmatic which may be due to the fact that focusing/defocusing effects of irregular topography at the inner core boundary [Wen, 2006] or near the UIC/LIC boundary are not considered in the present study.

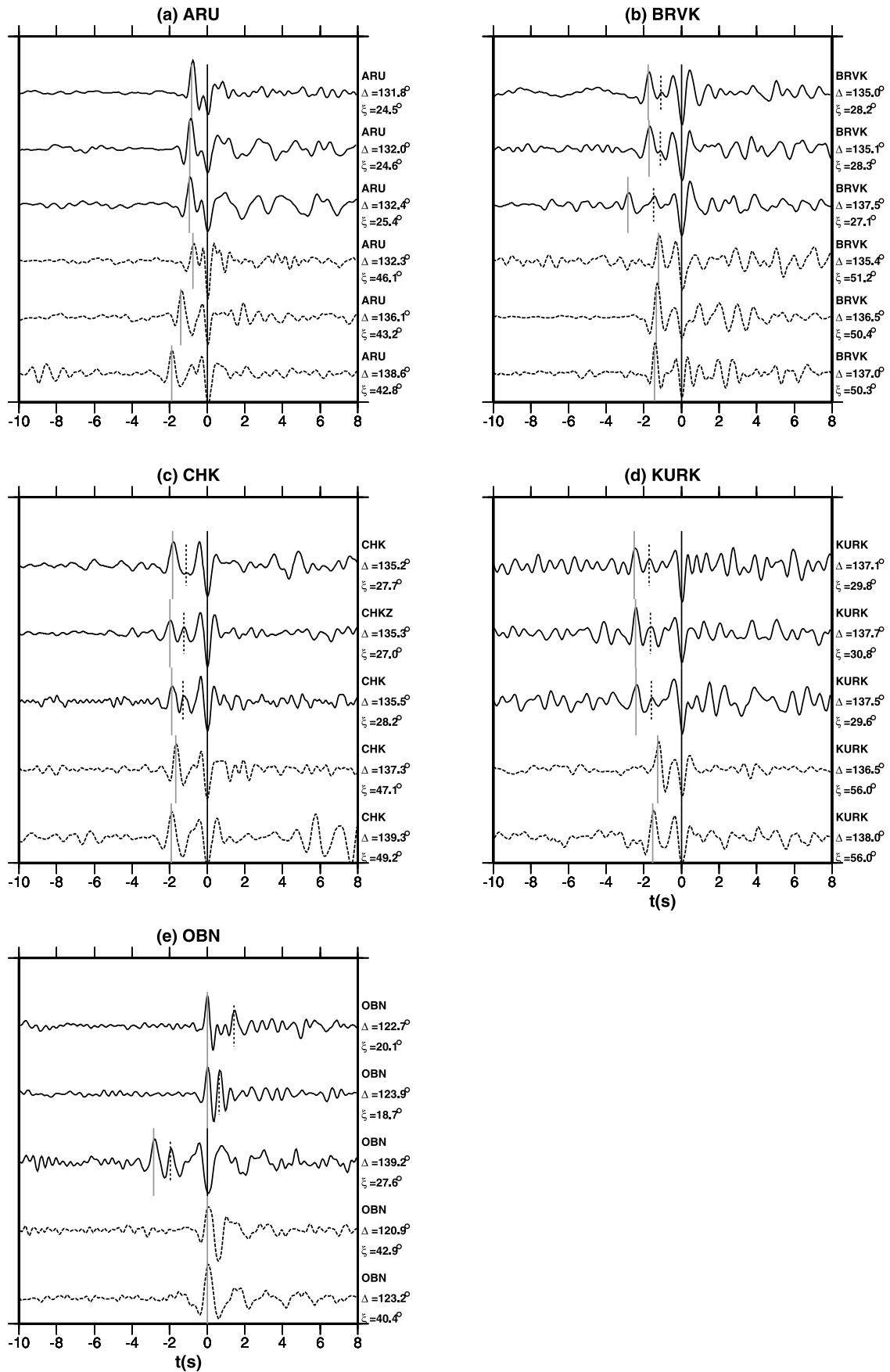


Figure 7

3.2.5. Region G4

[21] The polar PKiKP-PKIKP waveforms for the seismic data sampling region G4 show that (1) the PKiKP-PKIKP bifurcation is not observed at the distance range of 126° – 128° ; (2) the PKIKP phases arrive about 0.3 s earlier than the predictions based on PREM; and (3) the polar PKIKP amplitudes are smaller than the equatorial PKIKP amplitudes (Figure 8c). Non-observed bifurcation in the distance range of 126° – 128° constrains the top isotropic layer to be 30–50 km thick. Note that synthetics based on a velocity model with an isotropic layer of 30 km (G41 velocity model, black solid line in Figure 8a; G41 synthetics, solid traces in Figure 8d) and a velocity model with an isotropic layer of 50 km (G42 velocity model, black dashed line in Figure 8a; G42 synthetics, dashed traces in Figure 8d) can equally well fit the observations at the distance range of 126° – 128° . To explain the observed PKiKP-PKIKP waveforms at the distance range of 133° – 135° , G41 synthetics based on G41 velocity model with a 30-km-thick isotropic UIC would require a P velocity increase of 1.6% at the UIC/LIC boundary to explain the observations, while G42 synthetics based on G42 velocity model with a 50-km-thick isotropic UIC would require a P velocity increase of 2.2% at the UIC/LIC boundary to explain the observations. However, G42 synthetics can better explain the observed move-out and amplitudes of the triplications at the distance range of 133° – 135° (Figures 8c and 8d). Synthetics based on an attenuation model with a Q value of 600 in the UIC and a Q value of 200 in the LIC explain well the observed PKIKP amplitudes, with a Q value of 200 starting from either 30 km (G41 attenuation model, solid line in Figure 8b) or 50 km (G42 attenuation model, dashed line in Figure 8b) below the ICB.

[22] Beneath G4, the isotropic layer in the top of the inner core is about 30–50 km thick; the P velocity increase at the UIC/LIC boundary is about 1.6%–2.2%; and the attenuation structure has a Q value of 600 for the isotropic UIC and an average Q value of 200 for the anisotropic LIC (Figures 8a and 8b).

3.2.6. Regions G5 and G6

[23] Similar waveform characteristics are observed for the seismic data sampling regions G5 and G6. The polar PKiKP-PKIKP phases sampling region G5 show that (1) post PKIKP phases are observed at OBN at closer distances; (2) at the distance of 131° , the PKIKP arrivals are about -0.1 s to 0.2 s relative to PREM; and (3) the polar PKIKP amplitudes are larger than the equatorial PKIKP amplitudes (Figure 9c). The polar observations sampling G6 show that (1) no bifurcation is observed at the distance of 128° ; (2) at the distance range of 130° – 132° , the PKIKP phases arrive about -0.2 s to 0 s relative to PREM; and (3) at the distance

of 138° , the PKIKP phase arrives about 0.8 s earlier than the prediction based on PREM, and a post PKIKP phase is observed at OBN (Figure 10c).

[24] Examination of various records at same seismographs rules out the possibility that the above anomalous observations originated from the localized structure beneath seismograph. At station ARU, the polar PKIKP amplitudes (solid traces in Figure 7a) are larger than the equatorial PKIKP amplitudes (dashed traces in Figure 7a). The effects from the localized structure beneath ARU can thus be excluded. Same reasoning can also be applied to the post PKIKP phases recorded at OBN, in that the post PKIKP phases are observed uniquely for the polar path data (solid traces in Figure 7e) but not for the equatorial-path data (dashed traces in Figure 7e). These anomalous features are most likely caused by the triplications in the inner core.

[25] The available data for those sampling G5 and G6 can be used to place some bounds on the depth and magnitude of the UIC/LIC reflector and the attenuation structure. At closer distances, the move-out and amplitudes of the triplications relative to the PKiKP and PKIKP wave packages are diagnostic of distinguishing the depth of the UIC/LIC reflector. For instance, at the distance range of 120° – 128° , G41 synthetics based on a reflector placed at 30 km below the ICB show a steeper move-out and smaller amplitudes of the triplications than G42 synthetics based on a reflector placed at 50 km below the ICB (Figure 8d). The move-out of the triplications at OBN at the distance range of 122° – 123° in G5 and the PKiKP and PKIKP wave packages recorded at the FINES at the distance range of 124° – 128° in G6 constrain the UIC/LIC reflector to be 40 km below the ICB (Figures 9 and 10). The magnitude of the reflector and the velocity gradient below can be constrained by the subsequent move-out of the PKiKP-PKIKP phases. Synthetics based on a velocity model with a P velocity increase of 1.6% at the UIC/LIC boundary and the W2 velocity gradient below can match the PKiKP-PKIKP waveforms at the distance range of 130° – 138° and the time separation between the post PKiKP-PKIKP phases at OBN at the distance of 138° (Figures 9 and 10). The move-out of the triplications in the synthetics suggests that the large PKIKP amplitude observed at ARU at the distance of 131° results from the constructive interference between the triplications and the PKIKP phases (Figures 9c and 9d). Synthetics based on a layered attenuation model with a Q value of 600 in the 40-km-thick UIC and an average Q value of 400 in the LIC can match the observed PKIKP amplitudes at the distance of 138° in G6 (G6 attenuation model in Figure 10b, G6 synthetics in Figure 10d).

Figure 7. Observed PKIKP and PKiKP phases sampling along polar paths (solid traces) for several South Sandwich Islands earthquakes and those sampling along equatorial paths (dashed traces) for South America earthquakes recorded by five seismographic stations: (a) ARU, (b) BRVK, (c) CHK, (d) KURK, (e) OBN. The meaning of the bars is identical to those in Figure 6. Note that BRVK, CHK, KURK, and OBN consistently reveal the post PKIKP phases for those sampling along polar paths beneath G3, G4, G5, G6, but no such phases are observed for those sampling along equatorial paths. Note also that ARU exhibits large PKIKP amplitudes for those sampling along polar paths beneath G5 but relatively small PKIKP amplitudes for those sampling along equatorial paths.

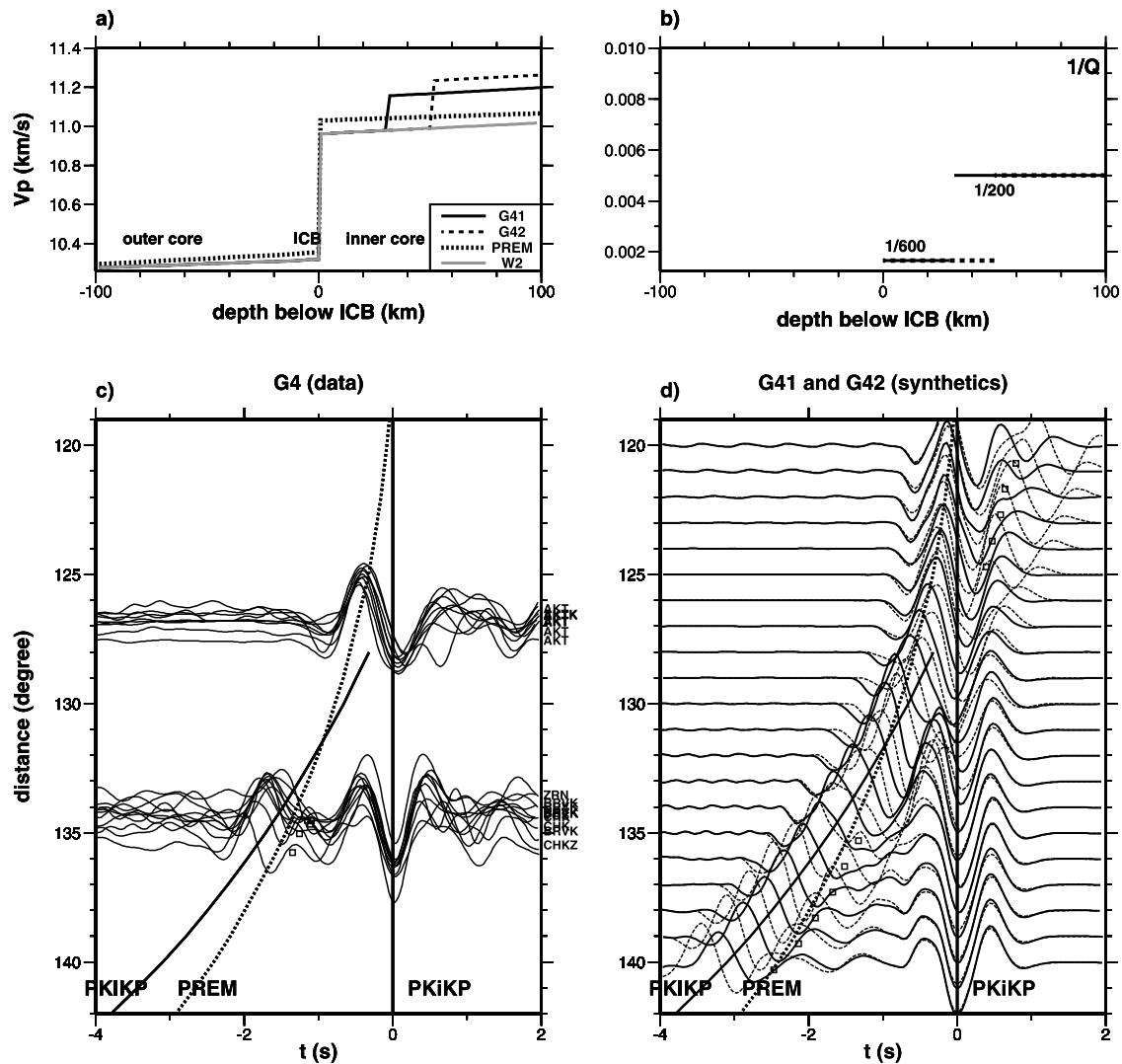


Figure 8. Seismic polar velocity (a) and attenuation (b) models near the ICB for region G4; observations of the PKiKP and PKiKP phases sampling G4 along polar paths (c); synthetics computed based on G41 (solid traces) and G42 (dashed traces) (d). The velocity model G41 has a 30-km-thick isotropic UIC, followed by a P velocity increase of 1.6% at the UIC/LIC boundary, and the W2 velocity gradient in the anisotropic LIC (black solid line in (a)); the attenuation model G41 has a Q value of 600 in the top 30 km and an average Q value of 200 in the LIC (solid line in (b)). The velocity model G42 has a 50-km-thick isotropic UIC, followed by a P velocity increase of 2.2% at the UIC/LIC boundary, and the W2 velocity gradient in the anisotropic LIC (dashed line in (a)); the attenuation model G42 has a Q value of 600 in the top 50 km and a Q value of 200 in LIC (dashed line in (b)). Distance corrections, synthetics, and the predicted PKiKP arrivals based on PREM (dotted line) and G41 (solid line) are made on the basis of a source depth of 600 km (c, d). At closer distances less than 130° , the observations and synthetics are aligned according to the predicted PKiKP arrivals based on PREM (dotted line). Because of the interference of the PKiKP and PKiKP phases, there appears an offset in aligning the later maximum amplitudes at closer distances. At larger distances, the observations and synthetics are aligned according to the maximum PKiKP amplitudes (c, d). The maximum amplitudes of the triplicated phases are marked by open squares.

[26] Beneath G5 and G6, the isotropic UIC is about 40 km thick; the P velocity increase at the UIC/LIC boundary is about 1.6%; and the attenuation model has a Q value of 600 for the 40-km-thick UIC and a Q value of 400 for the anisotropic LIC (Figures 9a, 9b, 10a and 10b).

3.2.7. Overall Polar Velocity and Attenuation Structures Beneath Africa

[27] Overall, in the top 80 km of the inner core beneath Africa, the thickness of the overlying isotropic UIC varies from 0 km (G1, G2) to 40–50 km (G4, G6), and the velocity increase from the isotropic UIC to the anisotropic

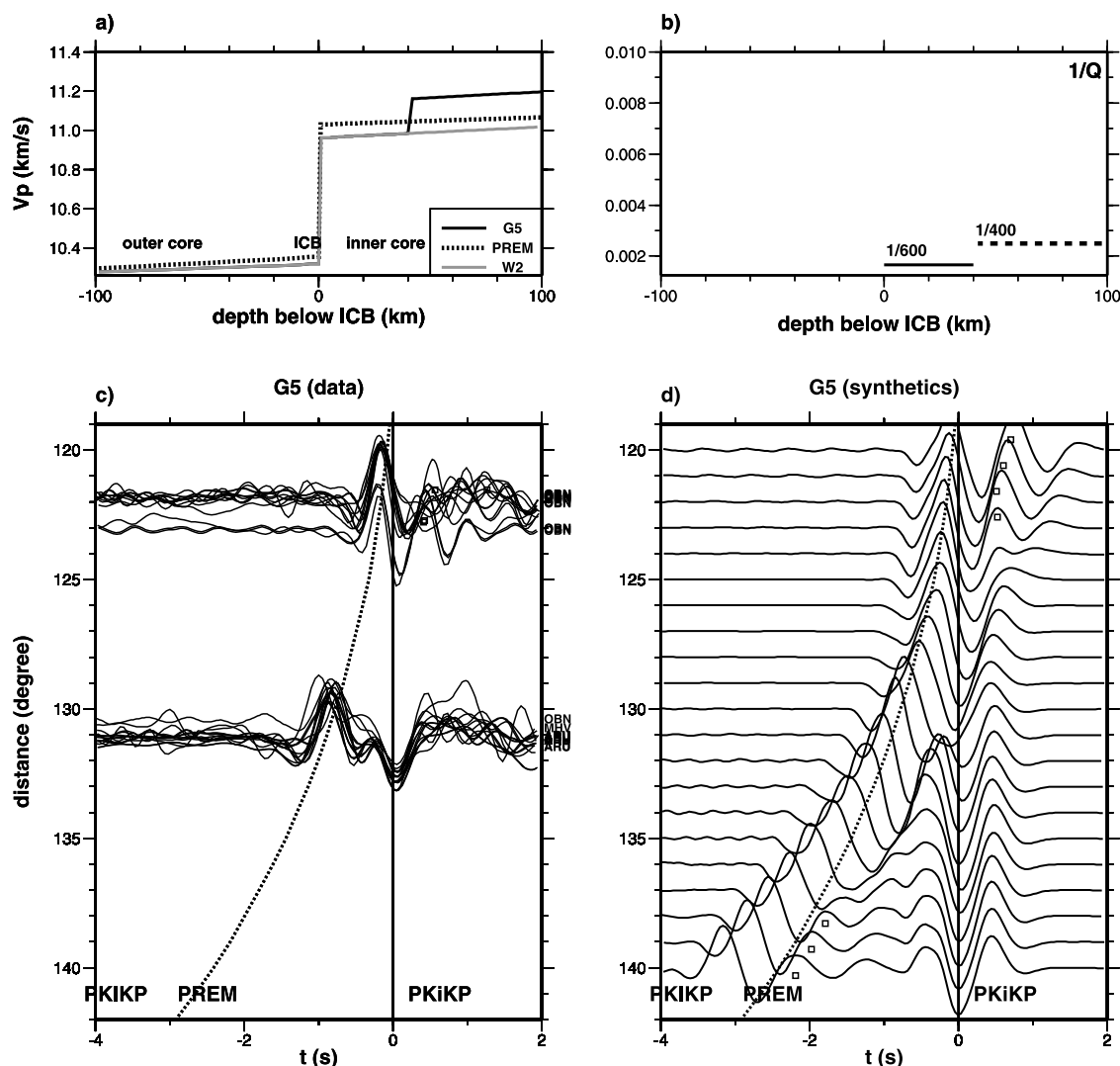


Figure 9. Seismic polar velocity (a) and attenuation (b) models near the ICB for region G5; observed PKiKP-PKiKP waveforms for the PKiKP phases sampling G5 along the polar paths (c); synthetic waveforms computed based on G5 (d). The velocity model G5 has a 40-km-thick isotropic UIC, followed by a P velocity increase of 1.6% at the UIC/LIC boundary, and the W2 velocity gradient in the anisotropic LIC (black solid line in (a)); the attenuation model G5 has a Q value of 600 in the top 40 km (solid line in (b)); the Q is assumed to be 400 in the LIC (dashed line in (b)). Distance corrections, synthetics, and the predicted PKiKP arrivals based on PREM (dotted line) are made on the basis of a source depth of 600 km (c, d). The observations and synthetics are aligned in the same way as those in Figure 8 (c, d). The maximum amplitudes of the triplicated phases are marked by open squares.

LIC changes laterally from 1.6% to 2.2%. The polar attenuation structures have a Q value of 600 for the isotropic UIC and Q values varying from 150 to 400 for the anisotropic LIC (Figure 11).

4. Discussions

4.1. Mantle Effects

[28] Seismic heterogeneities near the Earth's core-mantle boundary (CMB) affect little the PKiKP-PKiKP differential travel times. The Fresnel zone of the PKiKP and PKiKP phases is about 150 km at the CMB, but the spatial separation of this phase pair at the CMB is only 50 km. Seismic heterogeneities at the CMB would affect the PKiKP

and PKiKP phases in the same way. We adopt a recently developed three-dimensional global P -wave velocity mantle tomography model [Karason *et al.*, 2003] to estimate the mantle contributions on the PKiKP-PKiKP differential travel times. The predicted PKiKP-PKiKP differential travel time residuals based on this three-dimensional P -wave tomography model are about -0.02 s to $+0.04$ s, significantly smaller than the observed PKiKP-PKiKP differential travel time residuals.

[29] Dense observations sampling along various directions in the inner core but sampling same region at the CMB would also allow us to exclude the possibility that the observed PKiKP-PKiKP differential travel times and amplitudes are caused by the seismic heterogeneities in

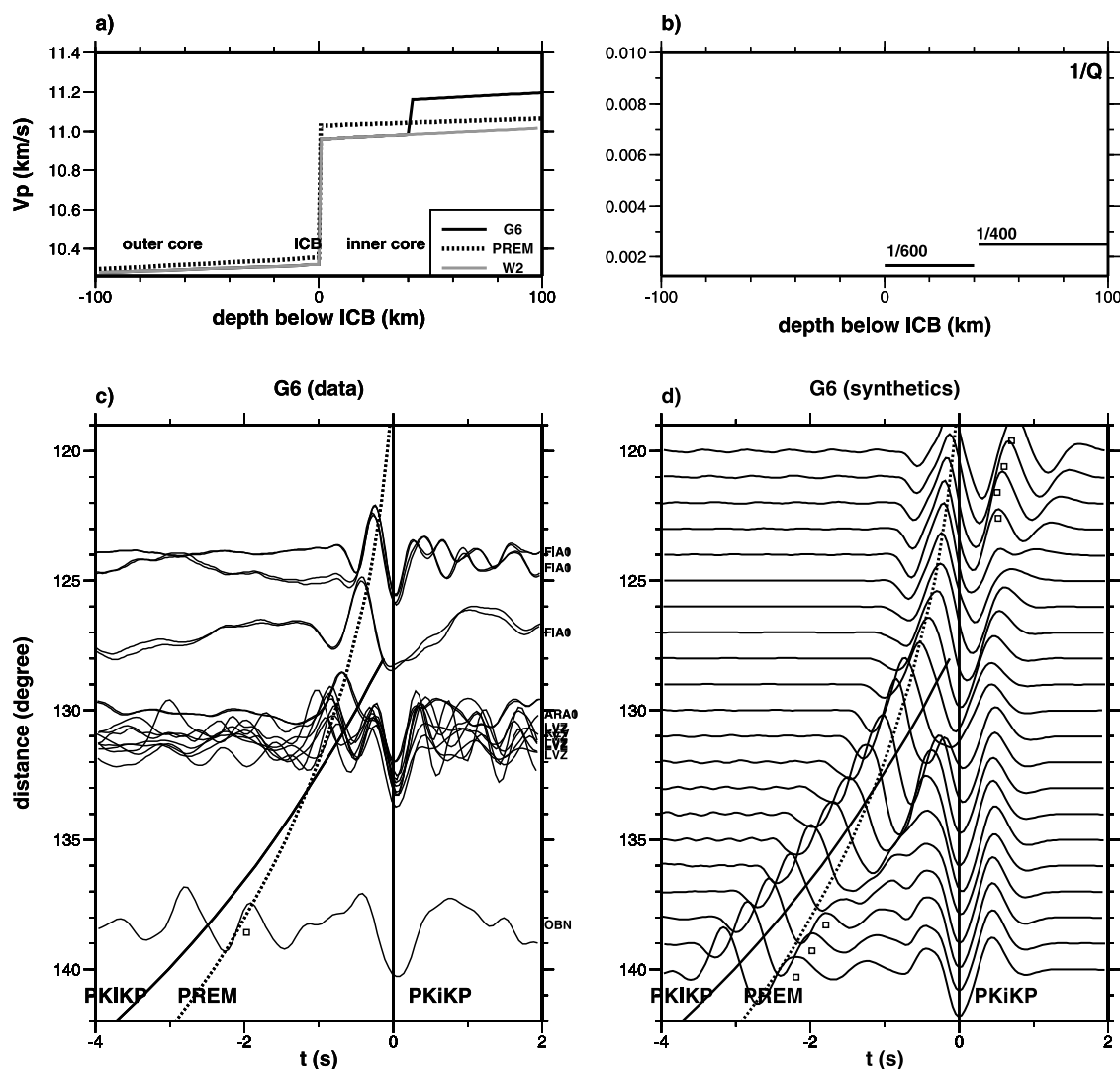


Figure 10. Seismic polar velocity (a) and attenuation (b) models near the ICB for region G6; observed polar PKiKP-PKiKP waveforms for the seismic data sampling G6 (c); synthetic waveforms computed based on G6 (d). The velocity and attenuation models of G6 are identical to those of G5 (a, b). Distance corrections, synthetics, and the predicted PKiKP arrivals based on PREM (dotted line) and G6 (solid line) are made on the basis of a source depth of 600 km (c, d). The observed and synthetic waveforms are aligned in the same way as those in Figures 8 and 9.

the mantle. For example, the receiver-side mantle is well sampled by both polar and equatorial PKiKP-PKiKP phases (Figure 12). If the seismic heterogeneities in the receiver-side mantle indeed perturbed the PKiKP-PKiKP travel times, same PKiKP-PKiKP travel time pattern would be observed for both the polar and equatorial data, opposite to our observations (Figure 12). The PKiKP and PKiKP entry points at the CMB are near the southern edge of a very low velocity province (VLVP) at the broad base of the “African Anomaly” reported by Wang and Wen [2004] (dotted contour in Figure 12b). However, the resolution of lateral location of the VLVP [Wang and Wen, 2004] and the Fresnel zones of the PKiKP and PKiKP phases indicate that the entry points of these seismic phases at the CMB lie in the distances far away enough from the VLVP for those seismic phases to be affected by the VLVP.

4.2. Comparison With Previous Studies

[30] Several previous studies investigated anisotropy in the deeper portion of the inner core beneath Africa using PKPbc-PKiKP phases [Souriau and Romanowicz, 1996, 1997; Souriau and Poupinet, 2003; Li and Richards, 2003]. Earlier studies by Souriau and Romanowicz [1996, 1997] suggested the existence of attenuation anisotropy beneath Africa, whereas more recent studies [Li and Richards, 2003; Souriau and Poupinet, 2003] suggested regional variations in velocity anisotropy in the LIC, mimicking those in the top 80 km of the inner core reported in this study. Li and Richards [2003] analyzed the differential travel times sampling eastern Africa (region G3) for several Novaya Zemlya nuclear explosions recorded by stations SNA and NVL in Antarctica and suggested strong anisotropy (3%) in the top 200 km of the inner core (their Figures 1 and 3). PKPbc-PKiKP phases do not resolve the seismic structures

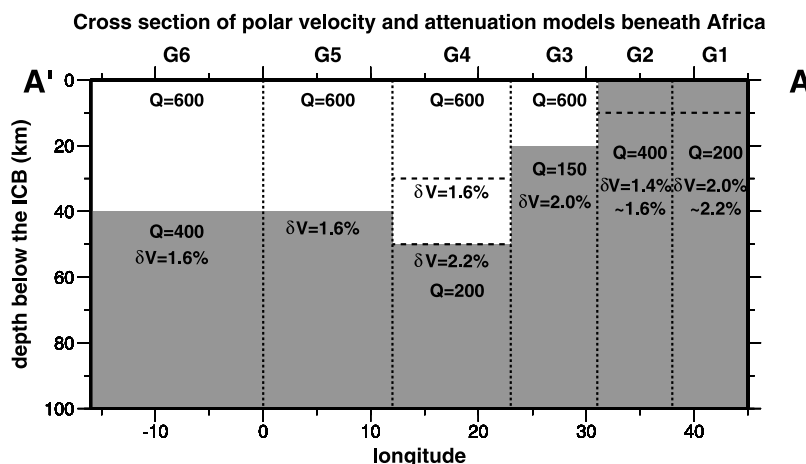


Figure 11. Cross section of the inferred polar velocity and attenuation models in the top 100 km of the inner core beneath Africa. The thickness of the isotropic UIC (white area) increases laterally from 0 km (G1, G2) to 40–50 km (G4, G6). The transition between the isotropic UIC and the anisotropic LIC (gray area) is sharp and varies laterally with P velocity increase from 1.6% to 2.2%. The attenuation structure for the isotropic UIC has an average Q value of 600, whereas the attenuation structure for the anisotropic LIC has Q values varying from 150 to 400. Cross section A-A' geographically corresponds to the profile along the gray dotted line in Figure 1.

in the uppermost 80 km of the inner core, but the predicted PKPbc-PKIKP travel times based on the extrapolation of G31 velocity model into deeper part of the inner core would explain the magnitude of their observed differential travel times. *Souriau and Poupinet* [2003] observed that the PKPbc-PKIKP travel times are very scattered for the South Sandwich Islands events recorded by station NRIL in Russia (sampling G5 and G6; their Figure 5). The predicted PKPbc-PKIKP travel times based on the extrapolation of G5 velocity model into deeper part of the inner core are about 1.2 s to 1.5 s smaller than the observations reported in their study. An increasing magnitude of velocity anisotropy at greater depths would explain their PKPbc-PKIKP differential travel times. A joint modeling of the PKPbc-PKIKP and PKiKP-PKIKP phases in the future should allow us to address anisotropy in the deeper portion of the inner core beneath Africa, as demonstrated in our recent study [Yu and Wen, 2006b].

4.3. Possible Interpretations

[31] Lattice preferred orientation of the anisotropic hexagonal closed packed (hcp) iron crystal has been advocated to explain the hemispheric variations in the inner core [Creager, 1999; Wen and Niu, 2002; Yu and Wen, 2006a]. A theoretical mineral physics study predicted that the anisotropy of the hcp iron single crystal, at the inner core condition, is about 10%–12% [Steinle-Neumann *et al.*, 2001]. It is plausible that the variations of the overlying isotropic thickness and deep anisotropy result from the different alignments of the anisotropic hcp iron crystals. Several other theoretical mineral physics studies suggested that the body centered cubic (bcc) iron may be stable at the core conditions with or without presence of sulfur and silicon, and that the layered UIC/LIC structure may result from the bcc-hcp solid phase transition [Vocadlo *et al.*, 2003, Belonoshko *et al.*, 2003]. While more quantitative analyses of the elastic and anelastic anisotropy of the bcc

phase at the inner core conditions and of the bcc-hcp-liquid phase boundary would be useful for interpreting our seismic results reported here, a large change of the UIC/LIC transition depth over small distances seems to suggest that the UIC/LIC boundary is inconsistent with a phase transition. Even if the bcc-hcp phase transition has a large Clapeyron slope, the temperature variation is small in the inner core and its transitional pressure (depth) would be expected to vary little, unless there is a major or minor composition dependence of the bcc-hcp phase transition and variations of those compositions exist in the top of the inner core. Alternatively, inclusion of partial melt has also been proposed to explain the observed anisotropy and high attenuation in the uppermost portion of the inner core [Singh *et al.*, 2000, Wen and Niu, 2002]. It is interesting to note that both a rapid change of the inner core boundary [Wen, 2006] and a complex anisotropy in the top of the inner core are observed beneath Africa. Such correspondence seems to suggest that the complex anisotropy may be explained by complex alignments of iron crystals resulting from a localized anomalous solidification of the inner core. Future interdisciplinary studies are warranted to understand the complex process of core formation and the resultant inner core anisotropy in this region.

5. Conclusions

[32] We analyzed the PKiKP-PKIKP data sampling the inner core beneath Africa along various directions to constrain the seismic anisotropy in the top 80 km of the Earth's inner core. The seismic waveforms are assembled from the recordings in the GSN and many regional seismic networks for the period of 1990–2005. The differential PKiKP-PKIKP travel times reveal polar-equatorial differences, indicating the presence of seismic anisotropy in the top 80 km of the inner core beneath Africa. The observations along the polar paths show complex regional variations

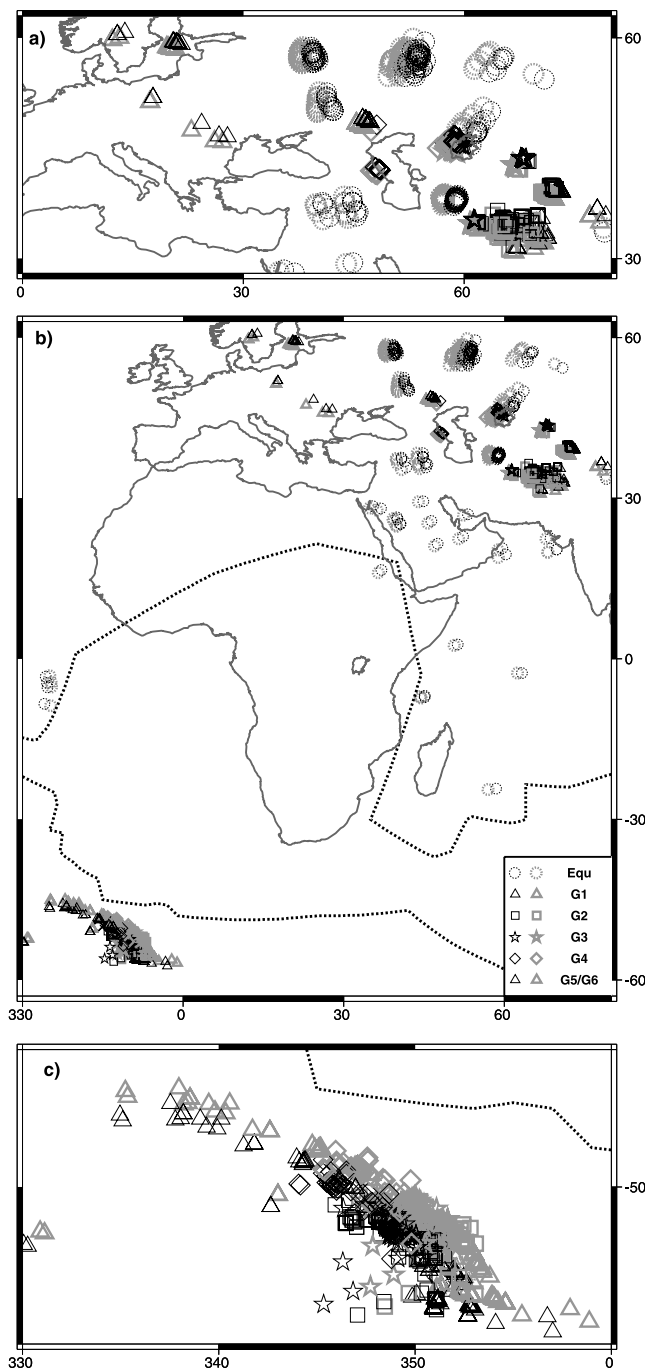


Figure 12. PKiKP and PKIKP entry and exit points at the CMB, with (b) showing the overview of the entire sampling region, and (a, c) showing blow-ups near the source-side CMB and receiver-side CMB, respectively. Black and light gray symbols represent the hit points at the CMB for the PKIKP and PKiKP phases, with their sizes of the symbols proportional to the sizes of the Fresnel zones of the short-period PKP waves at the CMB. Legend for different regions is shown in the inset in (b). Black dotted contour shows the boundary of the VLVP of the “African Anomaly” at the CMB [Wang and Wen, 2004].

across Africa: the differential PKiKP-PKIKP travel time residuals relative to PREM vary from 1.2 s for the PKIKP sampling eastern Africa, to -0.1 s for those sampling central Africa, and to -0.2 s to 0.8 s for those sampling western Africa. A correlation of small amplitude ratios with large differential travel time residuals is observed. The waveform data are spatially binned to constrain the regional dependence of velocity and attenuation anisotropy in the top 80 km of the inner core. Overall, in the top 80 km of the inner core across Africa, the thickness of the top isotropic layer varies from 0 to 50 km, and the P velocity increase across the UIC/LIC boundary fluctuates from 1.6% to 2.2%. The attenuation structure has a Q value of 600 for the isotropic UIC and 150 to 400 for the anisotropic LIC. The complex seismic anisotropy in the top of the inner core beneath Africa may be explained by complex alignments of the anisotropic hcp iron crystals, resulting from a localized anomalous solidification of the inner core.

[33] **Acknowledgments.** High-quality seismic waveforms were acquired from the GSN of the IRIS Consortium, GEOSCOPE, GEOFON, Kazakhstan, Kyrgyzstan, NORSAR, FINES, the New China Digital Seismograph Network, the Tien Shan Continental Dynamics, BLSF, SEDA, BANJO, CHARGE, and CNSN. Figures were prepared with the Generic Mapping Tools (GMT) software [Wessel and Smith, 1998]. We are also grateful to Robert van der Hilst and Chang Li for providing us their latest global three-dimensional mantle model. Discussions with Ken Creager, Don Helmberger, Xiaodong Song, and comments from Ken Creager, anonymous reviewer, and the Associate Editor were helpful in improving the manuscript. This work is supported by NSF grant EAR 0207746.

References

- Beghein, C., and J. Trampert (2003), Robust normal mode constraints on inner-core anisotropy from model space search, *Science*, *299*, 552–555.
- Belonoshko, A. B., R. Ahuja, and B. Johansson (2003), Stability of the body-centred-cubic phase of iron in the Earth's inner core, *Nature*, *424*, 1032–1034.
- Bergman, M. I. (1997), Measurements of elastic anisotropy due to solidification texturing and the implications for the Earth's inner core, *Nature*, *389*, 60–63.
- Bloxham, J., and D. Gubbins (1985), The secular variation of Earth's magnetic field, *Nature*, *317*, 777–781.
- Buffett, B. A., and H.-R. Wenk (2001), Texturing of the Earth's inner core by Maxwell stresses, *Nature*, *413*, 60–63.
- Cao, A., and B. Romanowicz (2004), Hemispherical transition of seismic attenuation at the top of the Earth's inner core, *Earth Planet. Sci. Lett.*, *228*, 243–253.
- Cormier, V. F., and A. Stroujkova (2005), Waveform search for the innermost inner core, *Earth Planet. Sci. Lett.*, *236*, 96–105.
- Creager, K. C. (1999), Large-scale variations in inner core anisotropy, *J. Geophys. Res.*, *104*, 23,127–23,139.
- Creager, K. C. (2000), Inner core anisotropy and rotation, in *Earth's Deep Interior: Mineral Physics and Tomography From the Atomic to the Global Scale*, *Geophysical Monograph 117*, edited by S.-I. Karato, A. M. Forte, R. C. Liebermann, G. Masters, and L. Stixrude, pp. 89–114, AGU, Washington, DC.
- Dziewonski, A., and D. L. Anderson (1981), Preliminary reference Earth model, *Phys. Earth Planet. Inter.*, *25*, 297–356.
- Garcia, R. (2002), Constraints on upper inner-core structure from waveform inversion of core phases, *Geophys. J. Int.*, *150*, 651–664.
- Garcia, R., and A. Souriau (2000), Inner core anisotropy and heterogeneity level, *Geophys. Res. Lett.*, *27*, 3121–3124.
- Helmberger, D. V. (1983), Theory and application of synthetic seismograms, in *Earthquakes: Observation, Theory and Interpretation*, edited by H. Kanamori, pp. 173–222, Soc. Italiana di Fisica, Bologna, Italy.
- Hulot, G., C. Eymin, B. Langlais, M. Manda, and N. Olsen (2002), Small-scale structure of the geodynamo inferred from Oersted and Magsat satellite data, *Nature*, *416*, 620–623.
- Ishii, M., and A. M. Dziewonski (2002), The innermost inner core of the Earth: Evidence for a change in anisotropic behavior at the radius of about 300 km, *Proc. Natl. Acad. Sci.*, *99*, 14,026–14,030.
- Jeanloz, R., and H.-R. Wenk (1988), Convection and anisotropy of the inner core, *Geophys. Res. Lett.*, *15*, 72–75.

- Karason, H., R. D. van der Hilst, and C. Li (2003), A new global model for 3-D variations in P wave speed in Earth's mantle, *Eos. Trans. AGU*, 84(46), Fall Meet. Suppl.
- Karato, S.-I. (1993), Inner core anisotropy due to the magnetic field-induced preferred orientation of iron, *Science*, 262, 1708–1711.
- Karato, S.-I. (1999), Seismic anisotropy of the Earth's inner core resulting from flow induced by Maxwell stresses, *Nature*, 402, 871–873.
- Li, A., and P. G. Richards (2003), Study of inner core structure and rotation using seismic records from Novaya Zemlya underground nuclear tests, in *Earth's Core: Dynamics, Structure, Rotation, Geodynamics 31*, edited by V. Dehant, K. Creager, S. Zatman, and S.-I. Karato, pp. 23–30, AGU, Washington, DC.
- Masters, G., and F. Gilbert (1981), Structure of the inner core inferred from observations of its spheroidal shear modes, *Geophys. Res. Lett.*, 8, 569–571.
- Morelli, A., A. M. Dziewonski, and J. H. Woodhouse (1986), Anisotropy of the inner core inferred from PKIKP travel times, *Geophys. Res. Lett.*, 13, 1545–1548.
- Niu, F., and L. Wen (2001), Hemispherical variations in seismic velocity at the top of the Earth's inner-core, *Nature*, 410, 1081–1084.
- Niu, F., and L. Wen (2002), Seismic anisotropy in the top 400 km of the inner core beneath the "eastern" hemisphere, *Geophys. Res. Lett.*, 29(12), 1611, doi:10.1029/2001GL014118.
- Ouzounis, A., and K. C. Creager (2001), Isotropy overlying anisotropy at the top of the inner core, *Geophys. Res. Lett.*, 28, 4331–4334.
- Poupinet, G., R. Pilet, and A. Souriau (1983), Possible heterogeneity of the Earth's core deduced from PKIKP travel times, *Nature*, 305, 204–206.
- Romanowicz, B., X. Li, and J. Durek (1996), Anisotropy in the inner core: Could it be due to low-order convection?, *Science*, 274, 963–966.
- Shearer, P. M. (1994), Constraints on inner core anisotropy from PKP (DF) travel times, *J. Geophys. Res.*, 99, 19,647–19,659.
- Singh, S. C., M. A. Taylor, and J. P. Montagner (2000), On the presence of liquid in Earth's inner core, *Science*, 287, 2471–2474.
- Song, X. (1997), Anisotropy of the Earth's inner core, *Rev. of Geophys.*, 35, 297–313.
- Song, X. (2003), Three-dimensional structure and differential rotation of the inner core, in *Earth's Core: Dynamics, Structure, Rotation, Geodynamics 31*, edited by V. Dehant, K. Creager, S. Zatman, and S.-I. Karato, pp. 45–63, AGU, Washington, DC.
- Song, X., and D. V. Helmberger (1995), Depth dependency of anisotropy of Earth's inner core, *J. Geophys. Res.*, 100, 9805–9816.
- Song, X., and D. V. Helmberger (1998), Seismic evidence for an inner core transition zone, *Science*, 282, 924–927.
- Song, X., and X. Xu (2002), Inner core transition zone and anomalous PKP (DF) waveforms from polar paths, *Geophys. Res. Lett.*, 29(4), 1042, doi:10.1029/2001GL013822.
- Souriau, A., and G. Poupinet (2003), Inner core rotation: A critical appraisal, in *Earth's Core: Dynamics, Structure, Rotation, Geodynamics 31*, edited by V. Dehant, K. Creager, S. Zatman, and S.-I. Karato, pp. 65–82, AGU, Washington, DC.
- Souriau, A., and B. Romanowicz (1996), Anisotropy in inner core attenuation: A new type of data to constrain the nature of the solid core, *Geophys. Res. Lett.*, 23, 1–4.
- Souriau, A., and B. Romanowicz (1997), Anisotropy in the inner core: Relation between P -velocity and attenuation, *Phys. Earth Planet. Inter.*, 101, 33–47.
- Steinle-Neumann, G., L. Stixrude, R. Cohen, and O. Gulseren (2001), Elasticity of iron at the temperature of the Earth's inner core, *Nature*, 413, 57–60.
- Stroujkova, A., and V. F. Cormier (2004), Regional variations in the uppermost 100 km of the Earth's inner core, *J. Geophys. Res.*, 109, B10307, doi:10.1029/2004JB002976.
- Takahashi, T., and W. A. Bassett (1964), High-pressure polymorph of iron, *Science*, 145, 483–486.
- Tanaka, S., and H. Hamaguchi (1997), Degree one heterogeneity and hemispherical variation of anisotropy in the inner core from PKP (BC)-PKP (DF) times, *J. Geophys. Res.*, 102, 2925–2938.
- Tromp, J. (2001), Inner-core anisotropy and rotation, *Annu. Rev. Earth Planet. Sci.*, 29, 47–69.
- Vocadlo, L., D. Alfe, M. J. Gillan, I. G. Wood, J. P. Brodholt, and G. D. Price (2003), Stability of the body-centred-cubic phase of iron in the Earth's inner core, *Nature*, 424, 536–539.
- Wang, Y., and L. Wen (2004), Mapping the geometry and geographic distribution of a very low velocity province at the base of the Earth's mantle, *J. Geophys. Res.*, 109, B10305, doi:10.1029/2003JB002674.
- Wen, L. (2006), Localized temporal change of the Earth's inner core boundary, *Science*, 314, 967–970, doi:10.1026/science.1131692.
- Wen, L., and F. Niu (2002), Seismic velocity and attenuation structures in the top of the Earth's inner core, *J. Geophys. Res.*, 107(B11), 2273, doi:10.1029/2001JB000170.
- Wenk, H.-R., J. R. Baumgardner, R. A. Lebensohn, and C. N. Tome (2000), A convection model to explain anisotropy of the inner core, *J. Geophys. Res.*, 105, 5663–5677.
- Wessel, P., and W. H. F. Smith (1998), New, improved version of generic mapping tools released, *EOS Trans. AGU*, 97, 597.
- Woodhouse, J. H., D. Giardini, and X.-D. Li (1986), Evidence for inner core anisotropy from free oscillations, *Geophys. Res. Lett.*, 13, 1549–1552.
- Yoshida, S., I. Sumita, and M. Kumazawa (1996), Growth model of the inner core coupled with the outer core dynamics and the resulting elastic anisotropy, *J. Geophys. Res.*, 101, 28,085–28,103.
- Yu, W., and L. Wen (2006a), Inner core attenuation anisotropy, *Earth Planet. Sci. Lett.*, 245, 581–594.
- Yu, W., and L. Wen (2006b), Seismic velocity and attenuation structures in the top 400 km of the Earth's inner core along equatorial paths, *J. Geophys. Res.*, 111, B07308, doi:10.1029/2005JB003995.
- Yu, W., L. Wen, and F. Niu (2005), Seismic velocity structure in the Earth's outer core, *J. Geophys. Res.*, 110, B02302, doi:10.1029/2003JB002928.

L. Wen and W. Yu, Department of Geosciences, State University of New York at Stony Brook, Stony Brook, NY 11794-2100, USA. (lianxing.wen@sunysb.edu; yu@mantle.geo.sunysb.edu)